To cite this article: YU X, HU K Y. Influence of submarine's acceleration and deceleration on wake spectrum characteristics in stratified flow[J/OL]. Chinese Journal of Ship Research, 2022, 17(3). http://www.ship-research.com/en/article/doi/10.19693/j.issn.1673-3185.02490.

DOI: 10.19693/j.issn.1673-3185. 02490

Influence of submarine's acceleration and deceleration on wake spectrum characteristics in stratified flow

*YU Xiang, HU Kaiye**

College of Shipbuilding Engineering, Harbin Engineering University, Harbin 150001, China

Abstract: [**Objectives**] This paper seeks to grasp the influence of a submarine's acceleration and deceleration on its wake spectrum characteristics in stratified flow and provide a theoretical basis for submarine stealth. [**Methods**] The accuracy of CFD technology in simulating the motion of the submerged body making waves on the free surface is first verified, and then analyses are made of the wave-making on the free surface, its convergence and divergence field, and internal wave velocity field under the acceleration and deceleration of a real-scale submarine. By calculating the divergence of the velocity field of the free surface, the influence of submarine acceleration and deceleration on the free surface and jump layer is determined in depth. [**Results**] The results show that when the submarine is in unsteady motion, the shear wave and scattered wave distribution of the wake field are completely different from those under uniform motion. Combining the wave height and velocity divergence field, the acceleration and deceleration of the submarine causes the free surface convergence and divergence effect. [**Conclusions**] When the submarine depth and stratification mode are the same, the wake field disturbance, wave height and roughness can be reduced when the sub-marine decelerates, and the acceleration state can significantly increase the probability of near-field disturbances leading to the detection of the submarine.

Key words: stratified flow; maneuver; wake field; synthetic aperture radar (SAR); convergence and divergence

CLC number: U661.1

0 Introduction

The hydrodynamic wakes generated by submarines in the submerged state can mainly be divided into Bernoulli hump, Kelvin wake, turbulent wake, internal wave wake, and vortex wake. In the field of non-acoustic submarine detection, such hydrodynamic signals can be detected by remote sensing and radar images [1－4]. Among them, the Kelvin wake and the Bernoulli hump above the hull are highly recognizable in remote sensing images. Submarines can effectively suppress such signals by increasing the submerged depth or reducing the speed, thereby significantly reducing the probability of being detected.

The internal waves generated by submarine navigation in the stratified ocean are not easy to control for conventional methods. Because of their long duration and wide propagation range, a submarine's position can generally be detected by spaceborne or airborne synthetic aperture radar (SAR) around the clock even in bad weather, in rain, and at night, and the motion state, submerged depth, and location of the submarine can be deduced through scattered images. Voropayev [5-6] found that large-scale vortices could be generated by the maneuvering and navigation of a submarine in a continuous stratified flow back in 1999. The interaction between the hydrodynamic wave-making induced by the unsteady maneuvering and navigation of the submarine and sea

Received: 2021－08－12 **Accepted**: 2021－09－09

Supported by: National Natural Science Foundation of China (51779053)

Authors: YU Xiang, male, born in 1995, master degree candidate. Research interest: computational fluid dynamics. E-mail: 1030279961@qq.com

HU Kaiye, male, born in 1980, Ph.D., associate professor. Research interests: ship hydrodynamics and non-acoustic stealth of submerged bodies. E-mail: hukaiye@hrbeu.edu.cn

***Corresponding author**: HU Kaiye

surface waves is of great academic and engineering research significance in the field of non-acoustic submarine detection in the future. At present, the theoretical studies, numerical simulation, and experimental studies of submarine's wake characteristics almost all assume that submarines navigate at a constant speed and depth, whereas unsteady motion and submarine's maneuvering motion are rarely investigated.

This paper will use computational fluid dynamics (CFD) technology to quantitatively analyze the influence of a submarine's unsteady maneuvering mode on the sea-surface and internal flow fields in a highly stratified ocean environment. Moreover, the influences of the submarine's motion state and acceleration on its stealth performance will be examined to provide the relevant theoretical basis for non-acoustic submarine detection technology and the deduction of a submarine's motion state.

1 Theoretical model

In CFD numerical simulation, the various physical quantities at different times in different spaces are represented by the variables at the discrete points in the computational domain. On the basis of certain principles and methods, the relevant equations are built and solved by approximation to obtain the relationships of the field variables at various discrete points [7-8]. The flow process in a density-stratified flow obeys the laws of mass conservation and momentum conservation, and the density jump layer based on temperature stratification should also observe the law of energy conservation. In the field of hydrodynamic CFD numerical simulation, the Reynolds-averaged Navier-Stokes (RANS) equation is usually used to deal with fluid viscosity.

1.1 Governing equation of numerical simulation

The three conservation laws the fluid obeys are expressed by the relevant governing equations. In this section, energy conservation, mass conservation, and momentum conservation equations are used for the numerical simulation of the wake and flow field when a submarine navigates in different stratified ocean environments.

1) Mass conservation equation.

The mass of any fluid particle does not change with time in unit time, and the mass flowing into and out of the micro-element body is the same. Similarly, the increased fluid mass in the micro-element body can be regarded as equal to the fluid mass flowing into the micro-element body in the same amount of time, and it can thus be expressed as

$$\frac{\partial u}{\partial x}+\frac{\partial v}{\partial y}+\frac{\partial w}{\partial z}=0 \tag{1}$$

where u, v, and w are the components of the velocity vector $\boldsymbol{u}$ in the directions of the three axes x, y, and z.

2) Momentum conservation equation.

The resultant external force on a fluid is equal to the increase in the kinetic energy of the fluid per unit of time. The momentum conservation equation for an incompressible fluid is

$$\frac{\partial(\rho u)}{\partial t}+\mathrm{div}(\rho u\boldsymbol{u})=-\frac{\partial p}{\partial x}+\frac{\partial \tau_{xx}}{\partial x}+\frac{\partial \tau_{yx}}{\partial y}+\frac{\partial \tau_{zx}}{\partial z}+F_x \tag{2}$$

$$\frac{\partial(\rho v)}{\partial t}+\mathrm{div}(\rho v\boldsymbol{u})=-\frac{\partial p}{\partial y}+\frac{\partial \tau_{xy}}{\partial x}+\frac{\partial \tau_{yy}}{\partial y}+\frac{\partial \tau_{zy}}{\partial z}+F_y \tag{3}$$

$$\frac{\partial(\rho w)}{\partial t}+\mathrm{div}(\rho w\boldsymbol{u})=-\frac{\partial p}{\partial z}+\frac{\partial \tau_{xz}}{\partial x}+\frac{\partial \tau_{yz}}{\partial y}+\frac{\partial \tau_{zz}}{\partial z}+F_z \tag{4}$$

where ρ is the fluid density; p is the pressure on the fluid micelle; τ_{xx} is the viscous stress in different tangential directions at different positions on the fluid micelle; F_x is the body force in various directions on the fluid micelle.

3) Volume of fluid (VOF) multiphase flow model.

For an incompressible fluid, the VOF equation obtained with the continuity equation $\nabla\cdot\boldsymbol{u}=0$ is

$$\frac{\partial C}{\partial t}+\nabla\cdot(\boldsymbol{u}C)=0 \tag{5}$$

$$C=\frac{C_\mathrm{f}}{C_\mathrm{u}} \tag{6}$$

where $\boldsymbol{u}$ is the fluid velocity; C_f is the volume of the fluid in the element; C_u is the volume of the element. When the calculated grid element is filled with the fluid, $C=1$; when no fluid is in the grid element, $C=0$; when $0<C<1$, the grids are fluid-surface grids.

1.2 Computational model and analysis method

1.2.1 Submarine acceleration and deceleration model

The acceleration during a submarine's speed-changing maneuvering process is usually variable, and its transient value is determined by various factors, such as the effective thrust and hydrodynamic parameters of the submarine propeller in this process. As such a value is extraordinarily complex to

solve in the numerical calculation [9-10] and many parameters cannot be obtained during the solution, the propeller is not taken into account during the acceleration and deceleration of the submarine in this paper. The average acceleration of the submarine in this process is solved by $a=(v_j-v_i)/t_{ij}$, where t_{ij} is the time of velocity variation; v_i is the velocity before velocity variation; v_j is the velocity after velocity variation. The transient velocity in the process of velocity variation is $aT + v_{(i-1)}$, where $v_{(i-1)}$ is the velocity of the previous data cycle and T is the time step of the calculation. It becomes stable after the submarine accelerates or decelerates to v_j. The field function with regard to the submarine's motion state is customized through programming during acceleration or deceleration.

1.2.2 Analysis method of wake field

The sensitivity of SAR is determined by the radar wave frequency. Setting the wave frequency to in the case of a low wind speed can eliminate the influence of the sea surface gust on the internal wave image, that is, the internal wave generated by submarine navigation can be detected from complex seaside signals. The United States effectively detected the internal wave signals generated by the navigation of the former Soviet Union's submarines at a submerged depth of 300 m. Combining theoretical research with experimental observation, Alpers et al. [11-12] revealed that regarding the signal intensity of convergence and divergence after wave-current modulation of the internal wave generated by submarine navigation and the sea-surface flow field, the range that can be detected and identified by SAR is 10^{-3}–10^{-4} s^{-1}, where s is the time unit second and used for all the measurement below. The spatial distribution characteristics of the sea-surface flow field induced by the internal wave generated by submarine motion are similar to those of the image of the internal wave on the water surface. A convergent flow appears before the wave crest and after the wave trough while a divergent flow appears before the wave trough and after the wave crest, that is, obvious divergent and convergent flows occur at the wave nodes of the image on the water surface.

In CFD, the convergent and divergent intensity of the flow field is the divergence of the horizontal velocity field $\boldsymbol{V}$ on the free surface, and it can be expressed as

$$\mathrm{div}(\boldsymbol{V}) = \frac{\partial u}{\partial x} + \frac{\partial v}{\partial y} \tag{7}$$

2 Case analysis

2.1 Numerical simulation verification

In this regard, the paper starts by verifying the reliability of the RANS equation, the SST k-ω turbulence model, and the VOF method in simulating the wake field when the submarine navigates in a submerged state and the accuracy of these methods in capturing the free surface. The free-surface wave-making characteristics when the Rankine ovoid model navigates in a submerged state at a constant speed are numerically simulated, and the results are compared with the wave-height data in the wave-making longitudinal section of the David Taylor Basin test conducted in 1966 [13] to verify the feasibility and accuracy of numerical simulation of submarine navigation.

A three-dimensional model of the Rankine ovoid is built by the software CATIA according to the geometric parameters of the ovoid [13] (Fig. 1). In this paper, the parameters are set with reference to the test data regarding submarine towing navigation in Taylor Basin. Specifically, the submerged depth of the model is set to 0.457 m, and the model is towed at a constant speed. The relevant numerical simulation is carried out under a speed of 3.048 m/s. For the computational domain, the length of the outflow section is set to 30.48 m, and the length of the inflow section is set to 1.219 m.

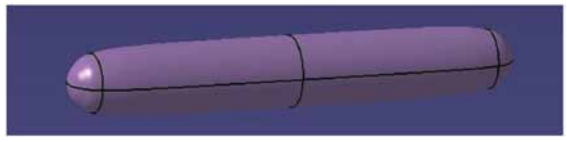

Fig. 1 Three-dimensional model of Rankine ovoid

The numerical simulation scheme for the flow field during the submerged navigation of the ovoid is verified by the software STAR-CCM +. The built-in cutting-body grid model of the software is adopted for grid division of the computational domain. Considering the viscous bottom layer, boundary layer grids are divided on the surface of the ovoid, and the grids along the wave height and wavelength directions on the sea surface are finely densified for sufficient numbers of grids in unit wavelength and wave height. The grid division is illustrated in Fig. 2.

In the case of a submarine with a submerged depth of 1.5 ft and a speed V = 10.0 ft/s, a stabilizing tendency of the flow field, and converging results, the data on the wave height in the sea-surface

(a) Overall grid division (b) Division of boundary layer grids on ovoid

Fig. 2 Grid division of computational domain for ovoid

longitudinal profile are compared with those of the Taylor Basin buoy test. As shown in Fig. 3 (where the wave height in the right part is in feet), the data on the wave height, waveform, and wavelength in the sea-surface longitudinal section obtained by the numerical simulation method in this paper are almost consistent with the results of the Taylor Basin test. This consistency indicates that the CFD method used in this paper is effective and accurate in capturing the wave-making characteristics on the sea surface when it is employed to simulate submarine motion. The CFD method is feasible for predicting the characteristics of submarine wake in the real ocean.

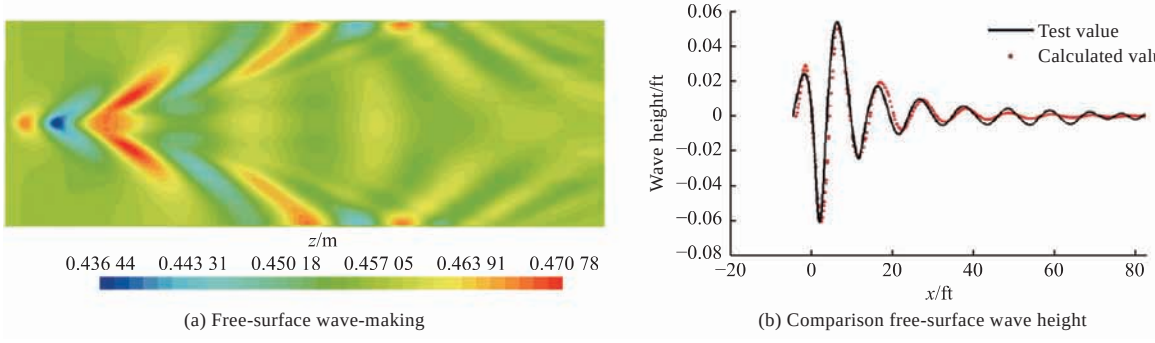

(a) Free-surface wave-making (b) Comparison free-surface wave height

Fig. 3 Numerical simulation verification

2.2 Computational model and working conditions to be calculated

A foreign conventional submarine with a length of 73.8 m and a width of 9.9 m is adopted as the computational model (Fig. 4). With a hull in a water droplet line shape, a bow rudder is arranged below the bow dome, and two horizontal and one vertical stern rudders are arranged at the stern.

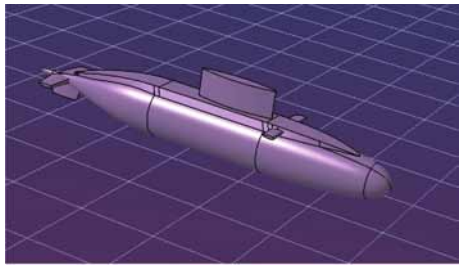

Fig. 4 Computational submarine model

The overset grid technology is employed for the numerical simulation of submarine motion at a constant depth and a variable speed. For the flow field, its top layer is defined as the air with a thickness of 15 m (under the condition of the sea surface air as the sea level). The fresh water in the middle layer is of a thickness of 40 m and a density of 997.56 kg/m^3, and the internal interface of the high stratification is 40 m below the free surface. The brine with a thickness of 110 m and a density of 1 024.2 kg/m^3 is taken below the internal interface. In the computational domain, the inlet is at 450 m in the inflow section, and the pressure outlet is at 1 000 m in the outflow section. The flow field is 500 m wide in the lateral direction. Cutting-body grids are used, and the interface grids are vertically densified to ensure that more than 30 vertical grids are present in the range of the wave height. Moreover, for the accurate characterization of the wavelength and waveform of the Kelvin wave on the sea surface, the free-surface grids are densified in a V-shaped double-layered manner, and more than 70 grids are set in the wavelength direction of the submarine's near-field. The total number of grids is about 25 million, and the grid division in different angles is shown in Fig. 5.

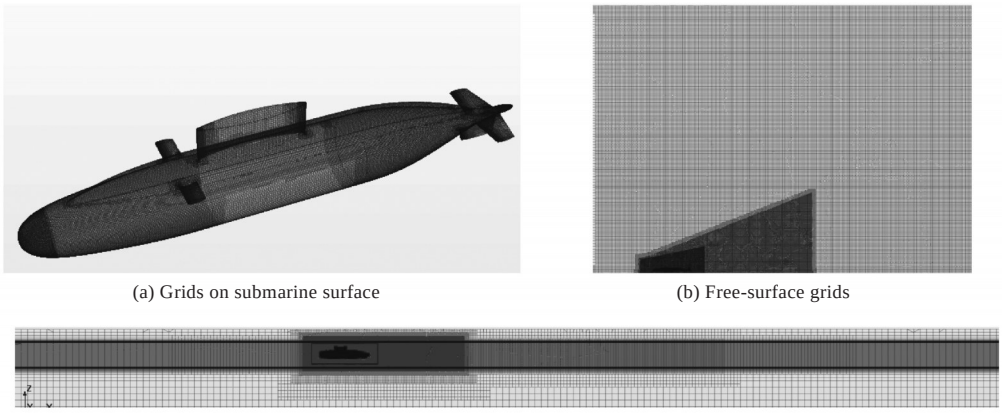

(a) Grids on submarine surface (b) Free-surface grids

(c) Grids in vertical flow field

Fig. 5 Grid division of computational domain for submarine

In this paper, the parameter selection for the numerical simulation in a density-stratified marine environment is based on the relevant hydrological data on China's inshore areas [14-15], and the environment is simplified as a highly stratified ocean model properly. The speeds are set to 12, 16, and 20 kn, respectively. The working conditions for acceleration and deceleration are direct navigation at a constant speed within 0−10 s, at a uniformly variable speed within 10−50 s after the flow field stabilizes, and at the speed at the time of 50 s within 50−60 s. The specific navigation parameters selected for each working condition are shown in Table 1.

2.3 Calculation results and analysis

For the submarine navigating at a constant speed of 12 kn, three sets of grids with different coarseness are divided, and the relative physical quantities are analyzed to verify the grid independence in the numerical simulation process. The numbers of the three sets of grids are 8.85 million (coarse), 25 million (medium), and 45 million (fine), respectively. The calculated wave-making is shown in Fig. 6 (the wave height and velocity fields in all working conditions in the following figure are in m). The analysis reveals that the maximum wave-making difference between the medium grids and the fine grids is within 5%. The medium grid scheme is finally selected on a comprehensive consideration of accuracy and calculation time.

Fig. 7 shows the waveforms of wave-making at the internal interface at t = 60 s when the submarine navigates at different speeds and in unsteady states. Under constant-speed working conditions, the

Table 1 Working conditions to be calculated

Working condition	Stratification mode	Speed range/kn	Acceleration time/s	Motion state	Submerged depth/m
A1	High stratification	12	0	Constant speed	20
A2	High stratification	16	0	Constant speed	20
A3	High stratification	20	0	Constant speed	20
B1	High stratification	12−16	40	Uniformly accelerating	20
B2	High stratification	16−12	40	Uniformly decelerating	20
B3	High stratification	12−20	40	Uniformly accelerating	20
B4	High stratification	20−12	40	Uniformly decelerating	20

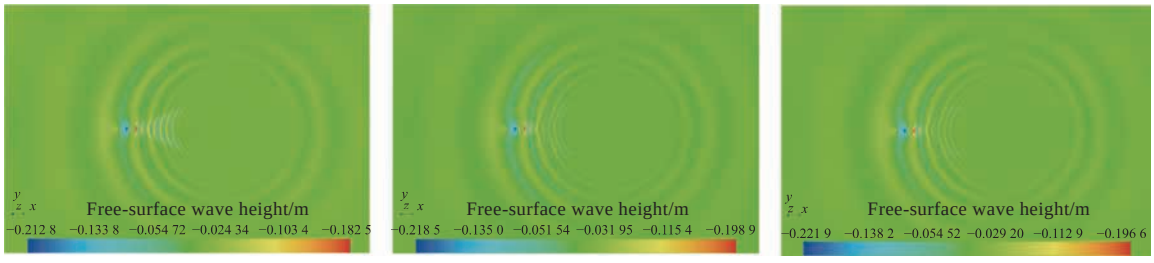

(a) 8.85 million grids (b) 25 million grids (c) 45 million grids

Fig. 6 Free-surface wave-making under different numbers of grids

wave-making distance at the internal interface increases significantly with the increase in speed. When the speed increases to 20 kn, the shear wave at the internal interface gradually becomes clear. The wave crest propagates in a towed manner and attenuates slowly, with its amplitude decreasing significantly with the increase in speed. Increasing slightly with speed, the wave trough has a scale the same as that of the hull and a stable state. The wave trough amplitudes of wave-making at t = 60 s under the accelerating working conditions B1 and B3 are slightly higher than that under the working condition A3, and the amplitude of the wave crest under these two working conditions is also higher than that under working condition A2. Compared with the constant-speed working conditions, the accelerating working conditions achieve similar waveforms and propagation laws, all in narrow V-shaped propagation to be exact, at the internal interface. A vortex can be observed at the end of the wave crest invariably, and its scale increases with speed. However, the amplitude in the range of the wave crest at

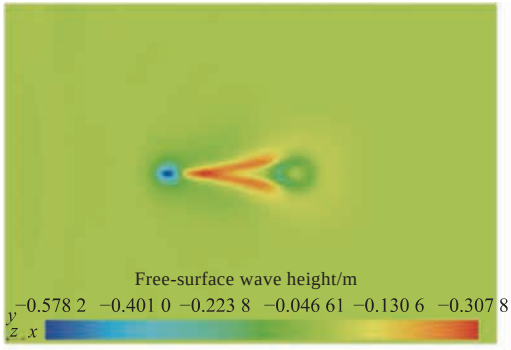

(a) Working condition A1: a speed of 12 kn

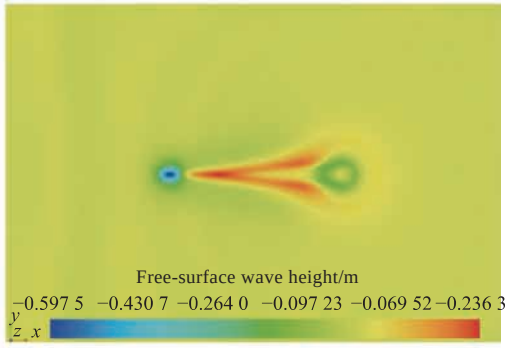

(b) Working condition A2: a speed of 16 kn

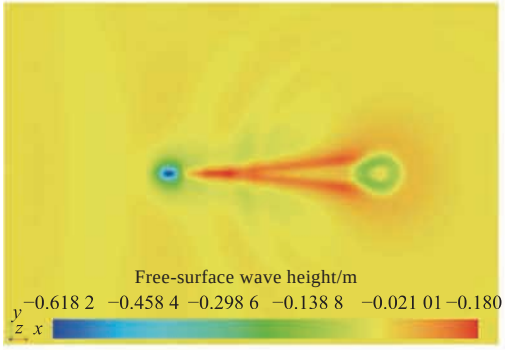

(c) Working condition A3: a speed of 20 kn

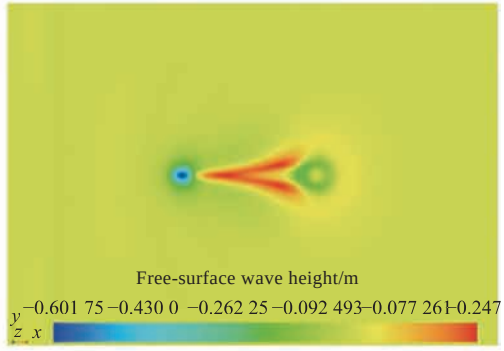

(d) Working condition B1: a speed of 12−16 kn

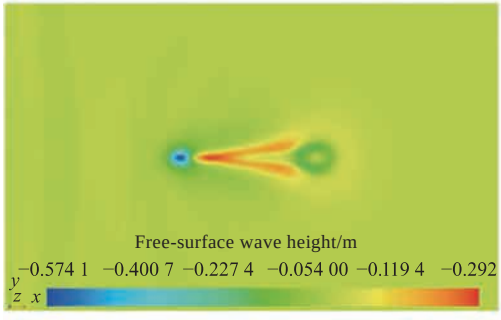

(e) Working condition B2: a speed of 16−12 kn

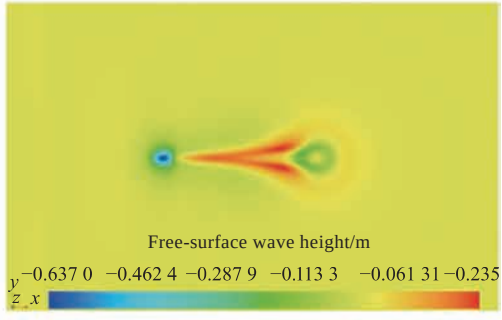

(f) Working condition B3: a speed of 12−20 kn

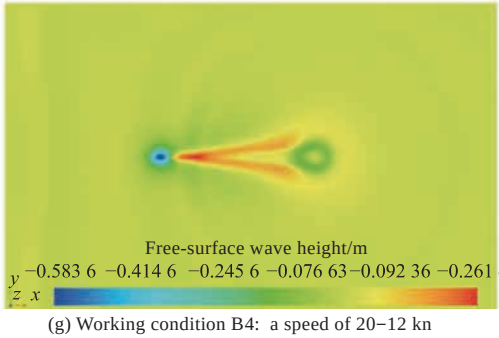

(g) Working condition B4: a speed of 20−12 kn

Fig. 7 Wave-making at the internal interface

the internal interface under accelerating working conditions is significantly higher than that under the constant-speed working conditions A2 and A3, and it decays more slowly to the rear. In contrast, the amplitude of the wave trough below the hull under the decelerating working conditions B2 and B4 is slightly smaller than that under the constant-speed working condition A2. The amplitude of the rear wave trough is only slightly larger in the near-field of the hull, and the attenuation to the rear is faster than that under the constant-speed and accelerating working conditions. The amplitude of the wave crest is higher than that under the working condition of a constant speed of 16 kn, and the scale of the vortex behind the wave crest is also smaller than that under the constant-speed and accelerating working conditions.

Fig. 8 shows the waveforms of free-surface wave-making at t = 60 s when the submarine navigates at different constant speeds and in unsteady states. When the submarine motion begins, the fluid around the submarine produces the Bernoulli hump

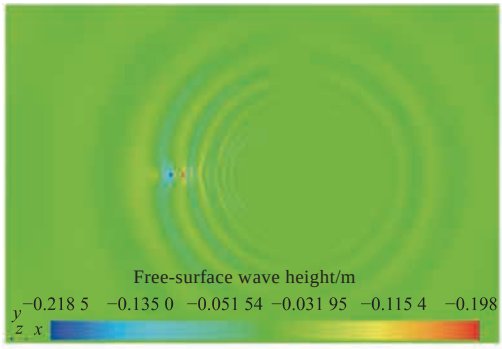

(a) Working condition A1: a speed of 12 kn

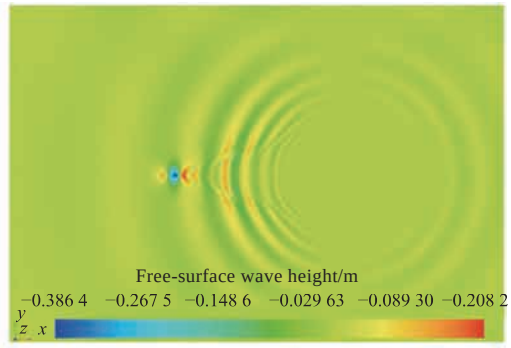

(b) Working condition A2: a speed of 16 kn

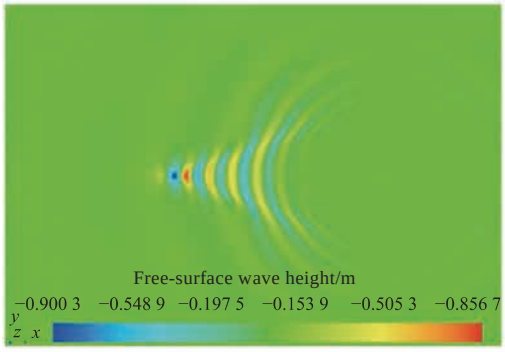

(c) Working condition A3: a speed of 20 kn

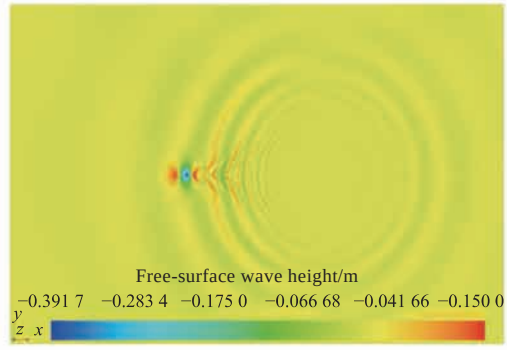

(d) Working condition B1: a speed of 12−16 kn

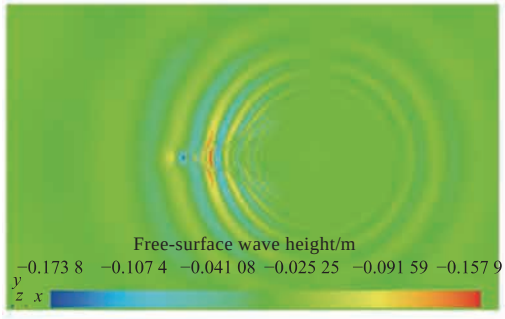

(e) Working condition B2: a speed of 16−12 kn

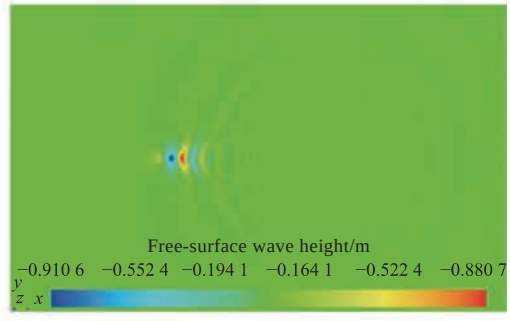

(f) Working condition B3: a speed of 12−20 kn

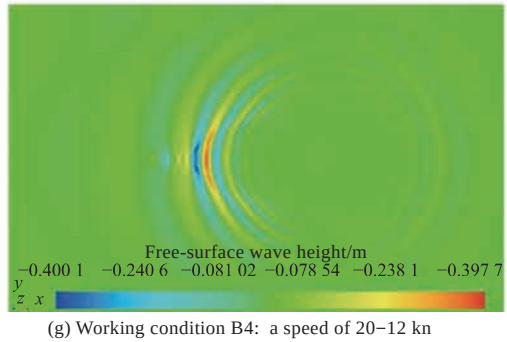

(g) Working condition B4: a speed of 20−12 kn

Fig. 8 Free-surface wave-making

due to the volume crowding-out effect of the submarine itself, and the wake corresponds to the first wave crest in the bow and the last wave trough in the stern, respectively. As submarine motion continues, the Bernoulli hump continues to develop backward and on both sides of the hull. Under a low speed (working condition A1), the wave-making behind the hull is mainly a shear wave; as the speed increases to 16 kn, the shear wave and the scattered wave on the free surface are both obvious; when the submarine's speed increases to a maximum of 20 kn, the free-surface wave-making is gradually dominated by the scattered wave. The free-surface wave-making is V-shaped under all working conditions, and the wave trough is invariably located above the submarine's command platform except under working condition B4. Under the constant-speed working conditions, the wavelength, wave height, and propagation speed of the wave-making increase significantly with speed, and the envelope angle of the scattered wave increases slowly with speed. Working condition B1 shows that when the speed is accelerated uniformly by 4 kn, the wave trough is around −0.392 m, which is about 2% higher than that under a constant speed of 16 kn, while the wave crest decreases by about 28%. Under this working condition, the scattered wave behind the hull is more obvious than that under a speed of 16 kn. When the speed is accelerated from 12 kn to 20 kn, the free-surface wave-making angle is smaller than that under working condition A3, and the free-surface wave-making is dominated by the Bernoulli hump in the hull's near-field. The wave-making behind the hull is obviously weak, with a wave height of wave-making about 2% higher than that under working condition A3 and slight increases in the amplitude of the wave crest and the wave trough. When the submarine decelerates from 16 kn to 12 kn, the wave height of free-surface wave-making is about 21% lower than that under working condition A1. When the submarine decelerates from 20 kn to 12 kn, the wave height of wave-making is about 55% lower than under working condition A3. In summary, deceleration can significantly reduce wave height in a short time. Under the accelerating working conditions in this paper, the wave-making wavelength gradually increases with speed. Under decelerating working conditions, it decreases with the decrease in speed, and the wavelength and wave-making at the bow are extremely sensitive to the change in speed. The free-surface wave-making angle slightly decreases during acceleration but increases significantly to a wide V-shape propagating to the rear of the hull during deceleration. Under the decelerating working conditions, the wave-making is more disorderly due to its superimposition caused by the wave speed difference in wave-making in the early and late periods.

For quantitative analysis of the free-surface wave-making characteristics, the wave-making section is taken at $y = 0$ (Fig. 9). When $t = 60$ s, the waveform of the free-surface wave-making in the submarine's near-field under working condition B1 is similar to that under a speed of 16 kn, and the maximum wave crest under these two working conditions is both located at the second wave crest. The wavelength under working condition B1 is shorter than that under the speed of 16 kn, and the wavelength of the rear wave-making is constantly changing. The submarine's maximum wave crest and trough are close to each other, and the wavelength becomes markedly smaller than that under the speed of 16 kn after the third wave trough. The subsequent waveform and the wave-making attenuation are both similar to those under the speed of 12 kn. The wave height and wavelength of free-surface wave-making in the submarine's near-field under other working conditions are close to those under the constant state of the final speed. The working conditions B1 and B2 show that the wavelength and wave height of wave-making increase with the increase in the submarine's speed during acceleration. The working conditions B2 and B4 indicate that the wavelength of wave-making under the decelerating working condition decreases gradually. Due to the low speed at the end of the navigation, the propagation speed of wave-making during the initial high-speed navigation is faster than that during the final low-speed navigation, resulting in the phenomenon of wave-making superposition and ultimate irregular waveforms of wave-making. In summary, regarding the submarine maneuvering and navigation at a variable speed and a constant submerged depth, the fluid in the near-field of the hull is affected by the volume crowding-out effect of the submarine. This effect is in turn affected by the submarine's speed and submerged depth. Consequently, the wavelength and wave height of the free-surface wave-making in the near-field are sensitive to the change in speed, and the submarine motion state can be determined from this perspective.

The three-dimensional free-surface convergence

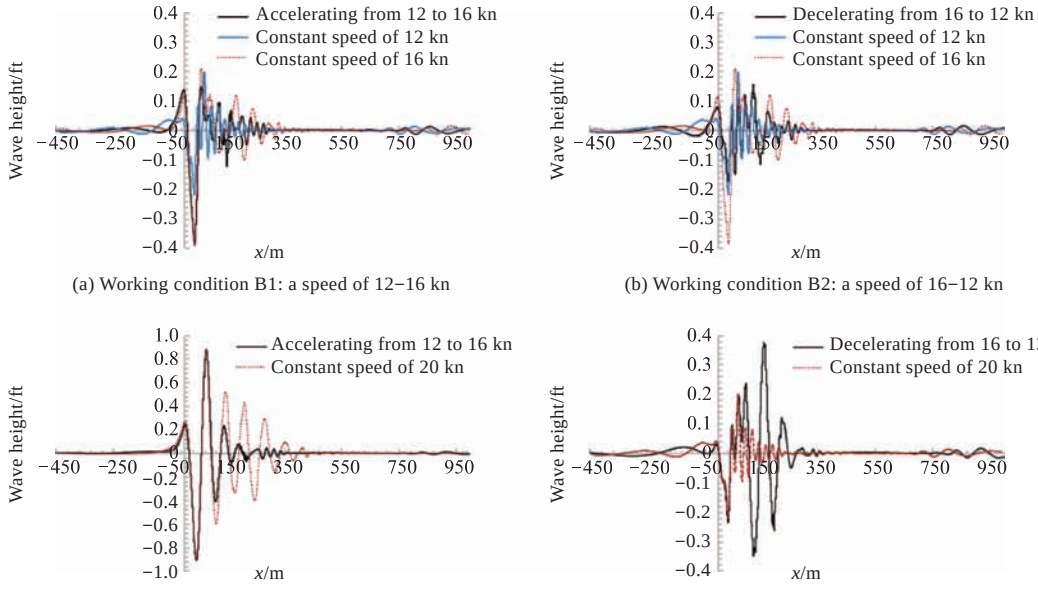

(a) Working condition B1: a speed of 12−16 kn

(b) Working condition B2: a speed of 16−12 kn

(a) Working condition B3: a speed of 12−20 kn

(b) Working condition B4: a speed of 20−12 kn

Fig. 9 Cross-sections of free-surface wave-making

and divergence intensities are used to represent the free-surface roughness. As shown in Fig. 10, the free-surface convergence and divergence intensities corresponding to the working conditions A1−A3 and B1−B4 fall within −0.0454−0.032 s^{-1}, −0.066−0.043 s^{-1}, −0.128−0.083 s^{-1}, −0.068−0.047 7 s^{-1}, −0.042 4−0.025 3 s^{-1}, −0.126−0.088 s^{-1}, and −0.058 2−0.045 4 s^{-1}, respectively. The above data show that regardless of the constant-speed, accelerating, or decelerating working conditions, the free-surface convergence peak is higher than the divergence peak. The difference between the two peaks increases with speed, and it increases significantly during acceleration and decreases during deceleration. The peaks are located on both sides of the maximum wave trough. When the submarine is accelerated from 12 kn to 16 kn under working condition B1, the free-surface roughness is slightly higher than that under the constant speed of 16 kn, and the roughness under the accelerating working condition B3 is also slightly higher than that under the constant speed of 20 kn. Regarding the decelerating working condition B2, the free-surface roughness is even smaller than that under the constant speed of 12 kn at 60 s. When the submarine is decelerated from a high speed of 20 kn to 12 kn under decelerating working condition B4, the free-surface convergence intensity and divergence intensity are about 55% and about 45% lower than those under the constant speed of 20 kn, respectively. In summary, under a constant submerged depth, acceleration will significantly improve the probability of submarine detection, while deceleration can significantly reduce this probability. When the submarine is decelerated below a speed of 16 kn, its stealth effect is obviously better.

To analyze the influence of the change in the submarine's motion state on its wake field, this paper takes the longitudinal section of the normal direction in the y direction at y = 0 m and sets a uniform velocity field range of 0−16 m/s, as shown in Fig. 11. Figs. 11(a) - (c) show that when the submarine's speed increases gradually, the submarine's command platform disturbs the velocity of the free-surface flow field greatly, and the disturbance increases gradually with the speed. The disturbance is particularly obvious at the speed of 20 kn. At this time, the disturbance caused by the command platform remains significant hundreds of meters behind the hull, and the attenuation is also relatively slow. When the submarine is accelerated from 12 to 16 kn under working condition B1, the wake field disturbance is even more serious than that under the constant speed of 16 kn, and the disturbance of the free-surface velocity field by the command platform is also significantly more serious than that under the working condition A2. When the submarine is slowed down from 16 to 12 kn under working condition B2, the disturbance of the free-surface velocity field in the near-field by the command platform is milder than that under the constant speed of 12 kn. Nevertheless, the far-field (200 m behind the hull) disturbance is slightly higher. The velocity disturbance at the stern is slightly higher than that un-

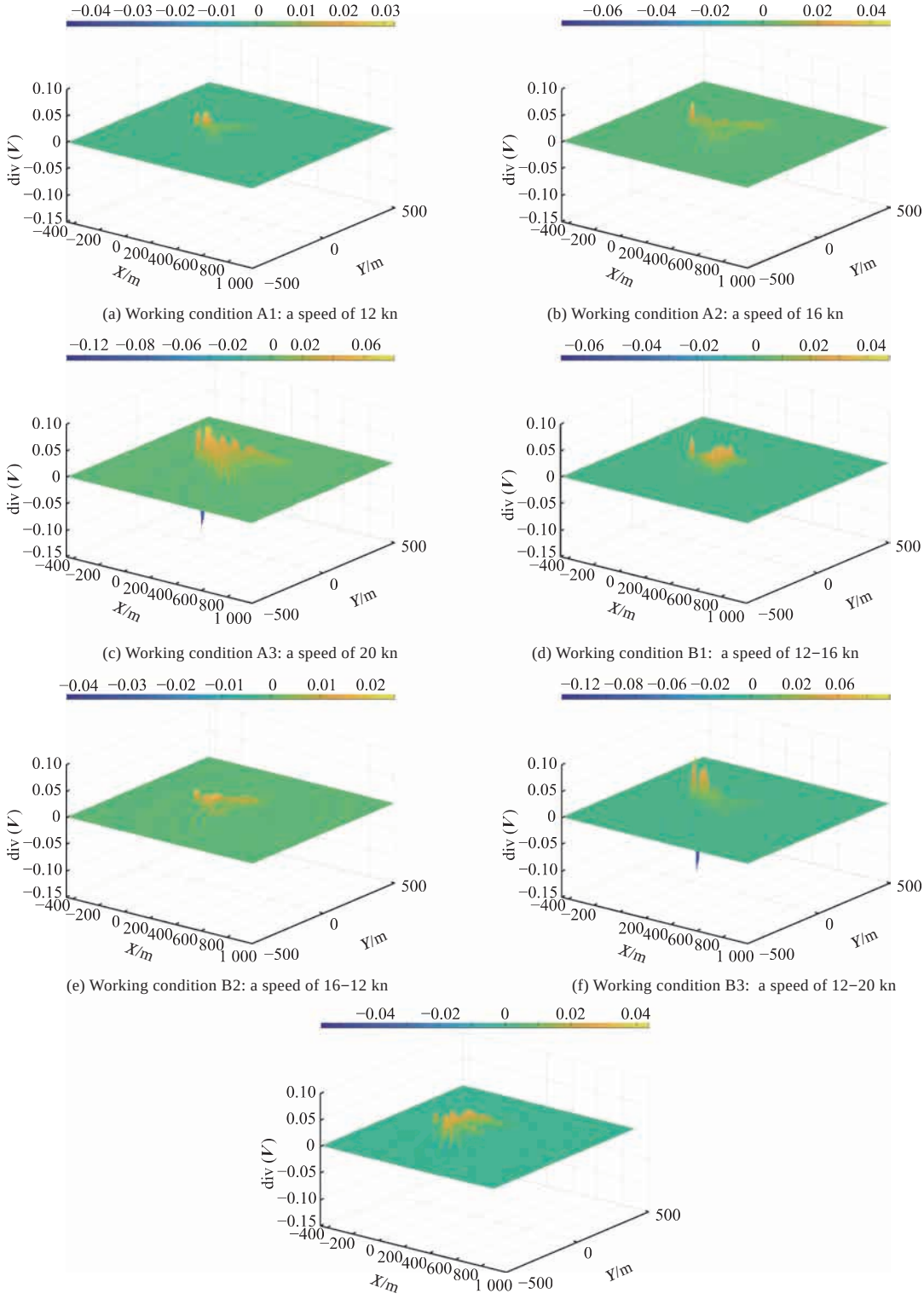

Fig. 10 Free-surface convergence and divergence intensities

der the constant speed of 12 kn but significantly lower than that under working condition A2. The distances of flow field disturbance behind the stern under working conditions B3 and B4 are similar. However, the near-field disturbance under working condition B3 is similar to that under working condition A3, and the disturbance at the end is obviously small due to the initial low speed. On the contrary, under working condition B4, the near-field disturbance is slightly lower than that under the constant speed of 12 kn, and the far-field disturbance is obviously more serious than that under the latter working condition. Clearly, in the same acceleration and deceleration ranges, the vertical scale of the vortex in the wake field when the submarine is in the deceleration state is significantly higher than that

(a) Working condition A1: a speed of 12 kn

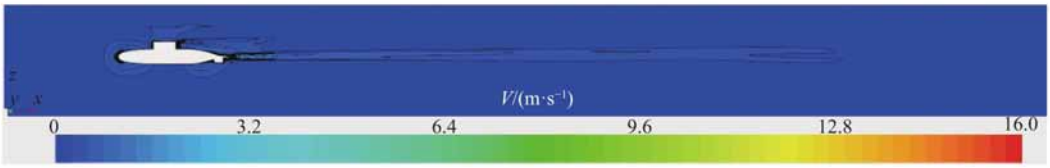

(b) Working condition A2: a speed of 16 kn

(c) Working condition A3: a speed of 20 kn

(d) Working condition B1: a speed of 12−16 kn

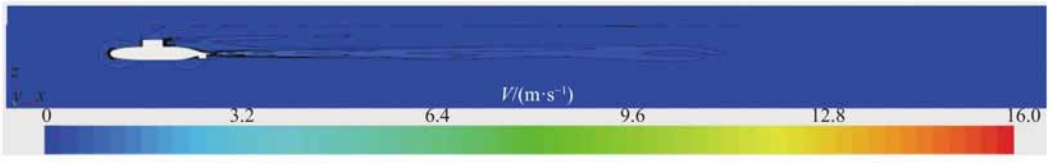

(e) Working condition B2: a speed of 16−12 kn

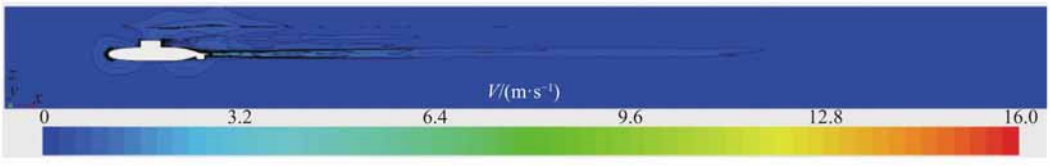

(f) Working condition B3: a speed of 12−20 kn

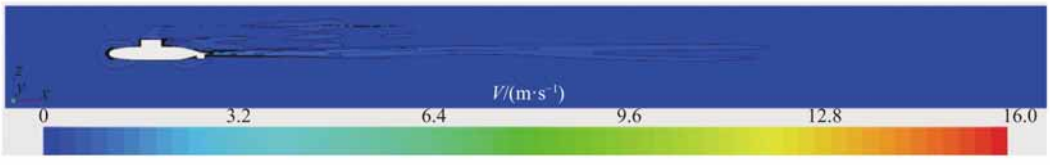

(g) Working condition B4: a speed of 20−12 kn

Fig. 11 Distribution of vertical velocity field

when it is in the acceleration state.

The velocity field distribution at the internal interface is examined to study the disturbance of the internal wave velocity field by the submarine's motion state (Fig. 12). The velocity field disturbances under the various working conditions are all extraordinarily severe in the near-field of the bow and stern. Under a constant speed, the horizontal propagation distance of the internal wave increases with speed. When the speed is 16 kn, the shear wave behind the hull becomes gradually obvious, and the shear wave increases more saliently with the speed. During acceleration, the horizontal propagation range near the hull increases slightly, and the far-field propagation distance is small in both cases. In deceleration, the horizontal propagation range of the internal wave in the submarine's near-field is obviously higher than that under the maximum constant speed. The shear wave at the internal interface during deceleration is weak in the front and strong in the rear, which is opposite to that under the accelerating working condition. Notably, unsteady ma-

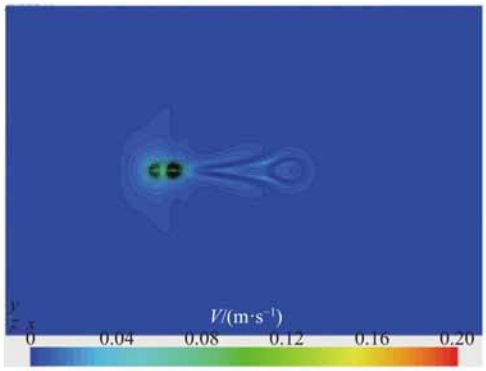

(a) Working condition A1: a speed of 12 kn

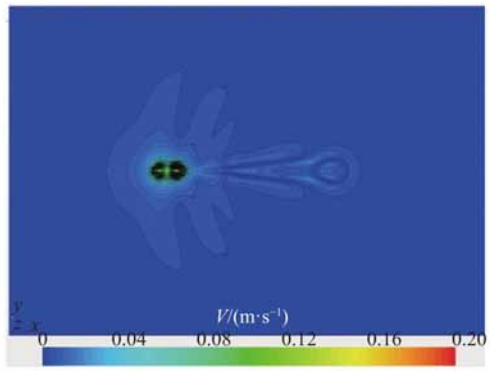

(b) Working condition A2: a speed of 16 kn

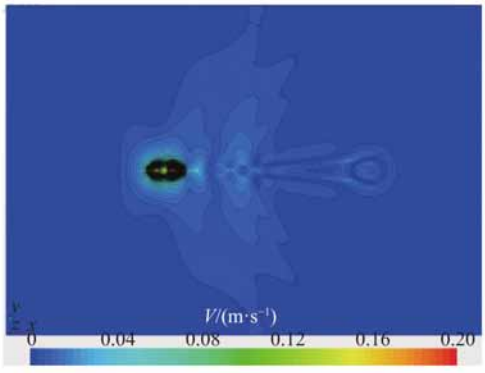

(c) Working condition A3: a speed of 20 kn

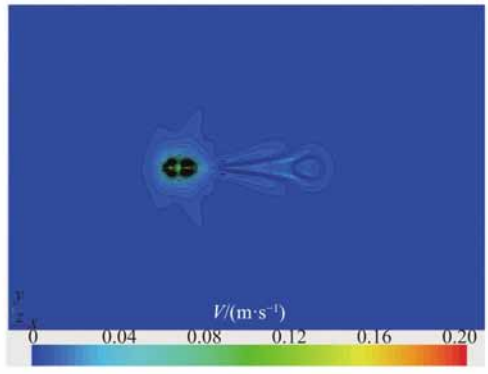

(d) Working condition B1: a speed of 12−16 kn

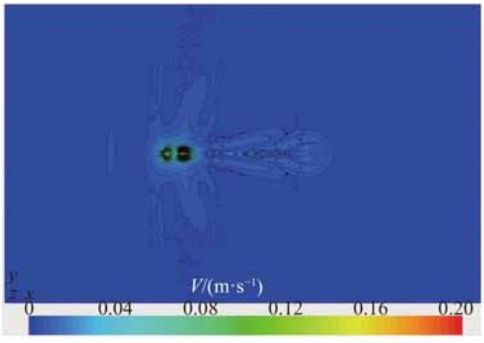

(e) Working condition B2: a speed of 16−12 kn

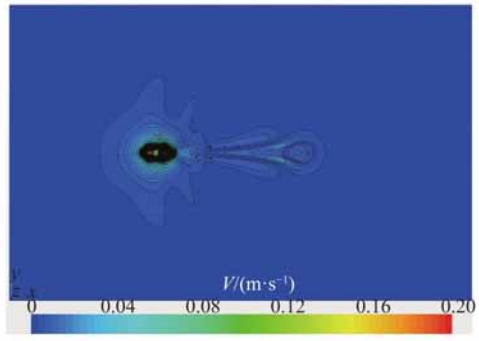

(f) Working condition B3: a speed of 12−20 kn

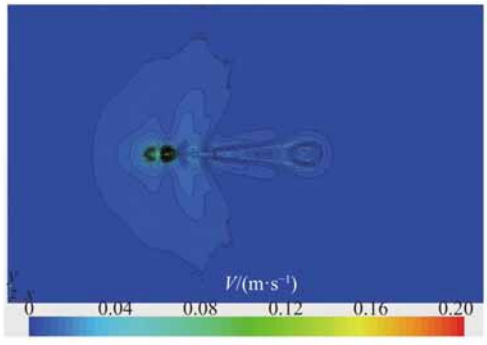

(g) Working condition B4: a speed of 20−12 kn

Fig. 12 Velocity field distribution at internal interface

neuvering and navigation significantly affects the horizontal propagation of the internal wave in the near-field. The comparison with Fig. 11 reveals obvious wake collapse during deceleration. In summary, although deceleration can significantly reduce the wave height and sea surface roughness, it disturbs the ocean interior significantly over a wide range.

3 Conclusions

In this paper, the accuracy of numerically simulating the wave-making when the submarine is in a submerged state was verified by the CFD method with the RANS equation and the SST k-ω turbulence model. On this basis, the double-layered flow stratification of the highly stratified ocean model

was performed through the Euler multiphase flow, and the constant-speed direct navigation and variable-speed maneuvering of the submarine in the highly stratified ocean environment were numerically simulated. Taking non-acoustic detection and stealth of submarines as the objective, the paper investigated the wake field characteristics of free-surface wave-making and wave-making at the internal surface when the submarine is in different motion states and three different speed ranges. The submarine's stealth effect was also evaluated from the perspective of remote sensing (convergence and divergence intensities). Compared with the conventional velocity field analysis, this paper presented a more comprehensive analysis of a submarine in the maneuvering and navigation state from multiple perspectives on multiple levels. The results are as follows.

1) The numerical simulation results of the wave-making of the Rankine ovoid in the submerged state are of small errors to the test results. With physical models and a grid division method meeting the accuracy requirements of the free-surface wave-making of a submarine in a submerged state, this paper provides an important method for solving incompressible density-stratified flows. In addition, this paper verifies the grid independence of the numerical calculation of a real-scale submarine, and it can thus provide necessary numerical calculation verification for further numerical simulation of the stratified flow during the maneuvering navigation of submerged bodies.

2) Regarding the accelerating maneuvering of a submarine in a highly stratified ocean environment, the first wave crest and trough increase rapidly with speed, and the corresponding wavelength of wave-making increases gradually. Nevertheless, the relative wave height increases slowly. Clearly, the internal wave excited by the volume effect of the submarine responds quickly at the first wave crest and trough on the free surface, and the volume effect is greatly affected by speed. Regardless of the accelerating or decelerating working conditions, the wave crest amplitude of the wave-making at the internal interface decreases. The wave crest of the wave-making at the internal interface attenuates more slowly than that under constant speeds and attenuates faster during deceleration. When the acceleration is doubled, the divergent flow intensity roughly doubles. The submarine is easier to detect when it is accelerated from 12 to 20 kn than under the constant speed of 20 kn, so acceleration can significantly increase the probability of submarine detection. The disturbance of the whole wake velocity field by acceleration is even more serious than that under the maximum constant speed.

3) Deceleration from a low speed (16 kn) can significantly reduce the amplitude of free-surface wave-making and sea surface roughness. The wave crest during acceleration and deceleration appears at different positions relative to the submarine. It is located at the head of the scattered wave crest during deceleration and at the tail of the scattered wave crest during acceleration. When the submarine is decelerated from a high speed, the wave height of wave-making and free-surface roughness are significantly lower than that under the maximum speed (20 kn). Nevertheless, the possibility of being detected is still high compared with that under the terminal constant speed of 12 kn. Therefore, deceleration from a low speed (16 kn) can effectively reduce the sea surface roughness. Deceleration causes a significantly smaller disturbance to the whole wake velocity field. Regardless of the accelerating or decelerating working conditions, the propagation distance of the internal wave in the hull's near-field increases. During deceleration, the increase is the most obvious, and the corresponding wake collapse in the near-field is also the most severe.

References

[1] MA W Z, DING Y, LI Y B, et al. On the numerical methods of the stable stratified flows and wake characteristics around a sphere [J]. Journal of Ship Mechanics, 2020, 24(10): 1278−1287 (in Chinese).

[2] DING Y, HAN P P, DUAN F, et al. Numerical study of linearly stratified flow past a cylinder based on a multiphase mixture model [J]. Journal of Harbin Engineering University, 2016, 37(9): 1179−1183 (in Chinese).

[3] DING Y, DUAN F, HAN P P, et al. Research on the relationship between moving patterns of submerged body and the features of induced internal waves in two layer fluid [J]. Journal of Ship Mechanics, 2016, 20(5): 523−529 (in Chinese).

[4] NIU M C, DING Y, MA W Z, et al. Research on the numerical simulation methods of continuously stratified flows based on thermal density current model [J]. Journal of Ship Mechanics, 2017, 21(8): 941−949 (in Chinese).

[5] VOROPAYEV S I, FERNANDO H J S. Wakes of maneuvering body in stratified fluids [M]. Progress in Industrial Mathematics at ECMI, Springer, 2010: 261−266.

[6] VOROPAYEV S I, MCEACHERN G B, FERNANDO

H J S, et al. Large vortex structures behind a maneuvering body in stratified fluids [J]. Physics of Fluids, 1999, 11(6): 1682−1684.

[7] WANG F J. Computational fluid dynamics analysis-software of CFD principles and applications [M]. Beijing: Tsinghua University Press, 2004: 7−10 (in Chinese).

[8] LI S Q, XIAO C R, CAO Z J. Numerical analysis of wake flow and hydrodynamics for a submarine based on STAR-CCM+ [J]. Chinese Journal of Ship Research, 2018, 13(S1): 29−35.

[9] ZHOU Z C, LIU Y H, LENG H P. Research of computer simulation on surface ship anti-submarine defense imitative training [J]. Computer Simulation, 2002, 19 (3): 1−4 (in Chinese).

[10] CHEN J H. The theory and practice of naval combat simulation [M]. Beijing: National Defense Industry Press,2002 (in Chinese).

[11] ALPERS W, HENNINGS I. A theory of the imaging mechanism of underwater bottom topography by real and synthetic aperture radar [J]. Journal of Geophysical Research: Oceans, 1984, 89(C6): 10529−10546.

[12] ALPERS W R, ROSS D B, RUFENACH C L. On the detectability of ocean surface waves by real and synthetic aperture radar [J]. Journal of Geophysical Research: Oceans, 1981, 86(C7): 6481−6498.

[13] SHAFFER D A. Surface waves generated by submerged rankine ovoids starting from rest [R]. Washington, DC: David Taylor Model Basin, 1966.

[14] LIU J F, MAO K X, ZHANG X J, et al. The general distribution characteristics of pycnocline of China Sea [J]. Marine Forecasts, 2013, 30(6): 21−27 (in Chinese).

[15] JIANG W, LI P, GAO W Y, et al. Pycnocline analysis on the Northwest Pacific Ocean [J]. Marine Forecasts, 2010, 27(2): 15−21 (in Chinese).

分层流中潜艇加减速对尾迹特征特性的影响

于祥,胡开业*

哈尔滨工程大学 船舶工程学院,黑龙江 哈尔滨 150001

摘　要:[**目的**]旨在研究分层流中潜艇加减速对尾迹特征特性的影响规律,为潜艇尾迹隐身提供理论依据。[**方法**]应用CFD技术,首先验证该技术模拟潜艇运动对自由面兴波的准确性,再基于自由面兴波与其辐聚辐散场、内波速度场进行分析,对实尺度潜艇进行加减速航行模拟。通过对自由面速度场求散度,深入研究潜艇加、减速对自由面及跃层的影响。[**结果**]研究表明:潜艇进行非定常运动时,尾流场横波、散波分布规律较匀速运动截然不同,其兴波夹角增减约10%~25%,且兴波峰值位置明显前置与后置,结合波高及速度散度场得到潜艇加、减速造成自由表面辐聚辐散效应的差异。[**结论**]当潜深和分层模式等相同,潜艇减速时,可降低尾流场扰动、兴波高度及其粗糙度,加速状态可显著增加潜艇近场扰动与被探测概率。

关键词:分层流;机动操纵;尾流场;合成孔径雷达;辐聚辐散